CFD-aided Military Ship Design and Helicopter Operation

Weixing Yuan[1], Alanna Wall[1], Eric Thornhill[2],
Chris Sideroff[3], Mahmoud Mamou[1], and Richard Lee[1]
1 Aerospace Research Centre, National Research Council Canada (NRC), Ottawa, Canada
2 Defence Research & Development Canada – Atlantic (DRDC-A), Halifax, Canada
3 Applied CCM Inc., Ottawa, Canada

Weixing.Yuan@nrc-cnrc.gc.ca

ABSTRACT

In support of Canadian industrial and defence ship design and offshore helicopter operations, a series of Ship Helicopter Operational Limits Analysis and Simulation (SHOLAS) projects are being conducted at the National Research Council Canada (NRC) in collaboration with Defence Research and Development Canada (DRDC). Part of the SHOLAS toolkit is a Canadian in-house capability to perform computational simulations of ship airwake using the open-source code OpenFOAM. This paper reports the challenges and lessons learned during the course of the projects. Two ship geometries were used for the validation exercise. The first was a highly simplified ship geometry called the simple frigate shape 2 (SFS2) which was used to validate the methodology for low-sea-state (static ship) cases. The second was a more complex configuration representative of a Canadian Patrol Frigate (CPF) which was used for testing more realistic high-sea-state (moving ship) conditions. Hybrid structured and unstructured grids were used because of the complexity of the CPF geometry. By employing delayed detached-eddy simulations (DDES), OpenFOAM was able to compute the unsteady ship airwake, and the results compared reasonably well to the available wind tunnel data and other references. The agreement between the computed and the experimental results was reasonable, which has provided confidence for the approach that was recently applied to another class of Canadian ship. Among other applications, computational fluid dynamics (CFD) airwake results can be used as input to produce representative airwake features in industrial high-fidelity piloted flight simulators.

1.0 INTRODUCTION

Objective: This paper aims to demonstrate the current capability of applying high-fidelity CFD techniques to industrial and defence ship design and shipboard helicopter operations including industrial flight simulators. Shipboard operations are among the most challenging of any piloting task for fixed or rotary wing aircraft (Polsky, 2006 and 2008; Forrest et al., 2012). The launch and recovery of helicopters are often performed from the landing decks of small ships, which are subject to random motion in six degrees of freedom. The difficulty is increased given that the landing deck is often immersed in the unsteady ship airwake. Because of the nature of bluff-body aerodynamics, the separated flow and sheared vortices interact and result in an unsteady airwake with highly turbulent structures which can significantly increase the difficulty associated with a helicopter launch and recovery manoeuvre. This work has applications for aircraft flight in complex flow fields beyond the ship airwake and is pertinent to other sectors of aviation industry.

Benefits: This technology is important for simulation of aircraft operations in complex flow fields created by bluff-body structures such as a ship superstructure or an urban landscape. Simulation provides a capability to test new ship and aircraft designs before building them, and has the potential to support the determination of the operational limits safely without relying on the wind and weather conditions (Polsky and Wilkinson, 2009;

Forrest and Owen, 2010). In commercial-flight applications, a level D aircraft simulator does not need to include complex flow fields because commercial aviation currently focusses on smooth flows and clear air turbulence, but simulators for specialized military applications need this kind of information. A key area that affects simulation fidelity is the modelling of ship airwake flows, which is not a trivial computational task. At-sea and wind tunnel measurements can be used to provide data from which airwake models can be generated. A major limitation with wind tunnels is that one cannot fully correlate flow fields in three dimensions since measurement techniques are usually point-wise or plane-wise sampling. At-sea flight testing is both labour and equipment intensive, requiring a dedicated ship and potentially multiple aircraft for days or weeks (Hodge et al., 2012). As a result, CFD is increasingly used for modelling ship airwake because the simulations can provide many correlated cloud grid points within the flow field and a number of simulations for different conditions can be performed at the same time to reduce testing time and costs. As unmanned aerial vehicles (UAVs) become more advanced, technology developments surrounding their use in urban environments are increasingly in demand. With increasing movement toward urban air mobility and because an urban wind environment has a lot in common with ship flows, likely CFD development and application will be required.

Barriers: The major technical barriers to a wider adoption of CFD for industrial flight simulations, both for shipboard and urban air applications, are accuracy, reliability, speed and affordability. The airflow past ships is normally at a low Mach number or nearly incompressible. A significant difficulty of incompressible flow calculations is that the continuity equation is not given in a time evolution form of density. Compressible flow solvers do not generally work well for flow simulation past ships because incompressible solutions converge quite slowly, especially when the grid is refined. As Ferziger and Perić (1996) pointed out, at high Mach numbers, the computing time increases almost linearly with the number of grid points as the grid size is increased. The exponent is approximately 1.1, compared to approximately 1.8 in case of incompressible flows, which results in costly and time consuming simulations for low-Mach-number or incompressible flows.

Capabilities and limitations: The airwake flow over the flight deck or in a city scape is massively separated and unsteady. The simulations must be time-accurate, which is time consuming and costly. Since military ships are large in size when compared to aircraft, the Reynolds number is of the order of 10^8. It is not feasible to resolve the flow past the ship using direct numerical simulations (DNS); however, it is unacceptable to perform the CFD simulations using an inviscid Euler solver for separated flows. Moreover, the superstructures of ships contain multiple bluff bodies. The flows past and around the multi-bluff body structures interact and often cause numerical instabilities. Furthermore, ship motion increases the difficulties in handling the grid motion in time-accurate CFD simulations. Because the ship airwake flow separation is mainly inertia-driven and the separation points are fixed by the model sharp edges rather than caused by boundary layer separation, DES is suitable for this kind of bluff-body aerodynamic flow. Although cities do not undergo motions, the geometry is more complex than a navy ship and therefore the challenges are similar.

Dependable and affordable high-fidelity CFD: In this study, sufficient accuracy and reliability were obtained through a rigorous validation process by combining the Canadian in-house computational, wind tunnel and sea-trial tests. To speed up the computations, parallel computing was employed using as many CPU cores as possible. The open-source software OpenFOAM was applied in this study, meaning that there was no restriction or costs to adding CPU power to the problem, which is a significant cost barrier when using commercial CFD codes for larger industrial and defence problems where additional license costs escalate with the numbers of CPU cores used.

Approaches to improve the fidelity of flight simulation: For commercial and defence simulator applications, the physics-based approach calculates the forces on the simulated aircraft by consulting a look-up table of the

flow information based on the CFD simulations. In parallel, we are developing engineering models to simplify the determination of the forces on the aircraft.

This paper documents the development of a CFD capability to calculate in a reliable and affordable manner ship airwake flows for industrial and defence shipboard helicopter operations. After a brief description of the CFD validation using the SFS2 (a simple frigate shape) data, investigations of a number of more realistic ship geometries are reported, including a number of challenges and subsequent lessons learned. At the end, in-flight simulator applications of ship CFD data are demonstrated. Further technology development will continue using the generic destroyer (DG), as proposed by Owen et al. (2020) and Wall et al. (2020).

2.0 CFD METHOD AND VALIDATION USING SFS2

The open-source CFD code, OpenFOAM, was applied to compute three-dimensional (3D) unsteady incompressible flows past ship models. The OpenFOAM pressure-based Navier-Stokes solver, *pimpleFoam*, was used in this study. OpenFOAM applies the integral form of the conservation laws of mass and momentum on a transparent (structured/unstructured) grid. A fully-implicit second-order temporal differencing scheme was implemented in the discretization. The discretization of the convective and diffusive fluxes was carried out in a co-located variable arrangement using a finite-volume approach, which was second-order accurate in space. The coupling of the pressure and velocity was handled using modified SIMPLE algorithms in the computations. OpenFOAM's *pimpleFoam* uses a hybrid PISO-SIMPLE (PIMPLE) algorithm, allowing for relatively large time steps. Because of the nature of the bluff-body aerodynamics, delayed detached eddy simulation (DDES) was employed to model the turbulence (Spalart et al., 2006).

To validate the CFD results, OpenFOAM (2014) was applied to SFS2 flow simulations. SFS2 is an updated version of the simple frigate shape (SFS) with a more elongated superstructure and pointed bow compared to the original SFS. The SFS is a conceptual standard ship design originally proposed by a ship airwake modelling working group within The Technical Co-operation Program (TTCP) to provide an easily repeatable benchmark case for validating CFD codes for ship airwake applications (Wilkinson et al., 1998). At full scale, the SFS2 is 455 feet long (138.68 m) and 45 feet (13.72 m) wide; details of the geometry are described by Zan (2005). Detailed numerical simulation and validation against wind tunnel data, including mean velocities, turbulence intensities, and power spectral density, were reported by Yuan et al. (2018a).

3.0 CHALLENGES AND LESSONS LEARNED

3.1 Complexity of ship geometry

The NRC has been supporting the Royal Canadian Air Force and Royal Canadian Navy in various aspects of helicopter operation in the airwake of the real-world Canadian Patrol Frigate (CPF) for many years. The first of the major challenges faced was the complexity of the ship geometry, which affected meshing and impacted the numerical stability. The computational setups were similar to those used in the SFS2 simulations. Because the smallest dimensions of some structures are 0.38 cm (0.15 in) for the real full-scale CPF, the simulations were performed at full scale to keep the original geometry without further modifications and solution values at a reasonable magnitude greater than machine zero. Owing to the complexity of the CPF superstructure features, unstructured grids were used near the ship (above water), except in the airwake where a structured grid was employed, as demonstrated in **Figure 1**a. This form of hybrid grid eased the mesh generation, in particular when the masts were included. The grid spacing in the ship airwake was 25 cm (10 in) at full scale, which was 20% smaller than the one used for the aforementioned SFS2 simulations (Yuan et al., 2018a), and thus comparable

to the spacing of the fine mesh used by Forrest and Owen (2010) for the SFS2 geometry. As a result, the final grid consisted of 61.2 million cells for the complete above-water ship with inclusion of the masts.

Difficulties were experienced when meshing the masts because they have over 13,000 entities (**Figure 1**b). The local spacing around the masts was determined according to the dimensions of the small structures, to ensure that every small structure had at least one control cell on its surface. Polsky (2004) mentioned that small geometric features such as antennae and masts can influence the turbulent wake signature behind large naval vessels. However, only the near wake immediately behind an antenna model was investigated in that work; the effect on the complete ship airwake was inconclusive. In order to evaluate the effects of the CPF masts on the ship airwake flows, two CPF configurations were used for the present CFD study – one with the original masts and the other with the masts omitted, as shown in **Figure 1**c and **Figure 1**d, respectively. As a result, the final grid consisted of 28.5 million cells for the no-mast case.

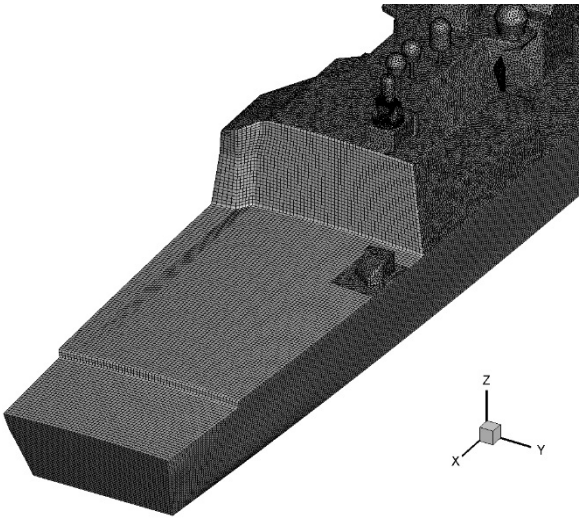

a) Surface meshes

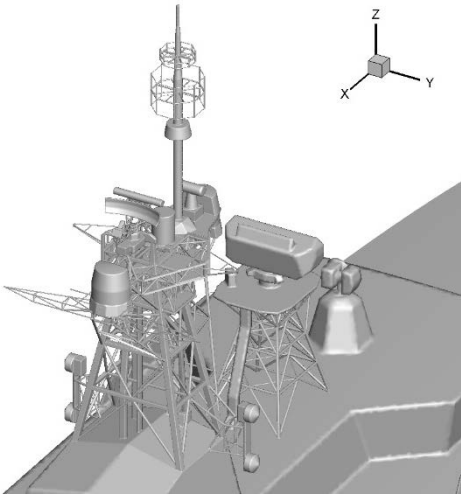

b) Masts

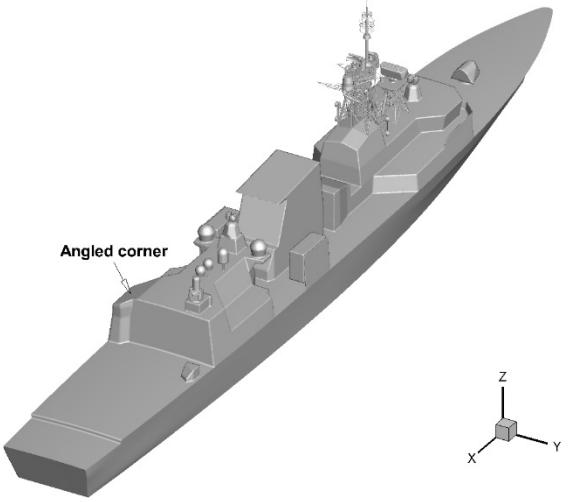

c) With-masts model

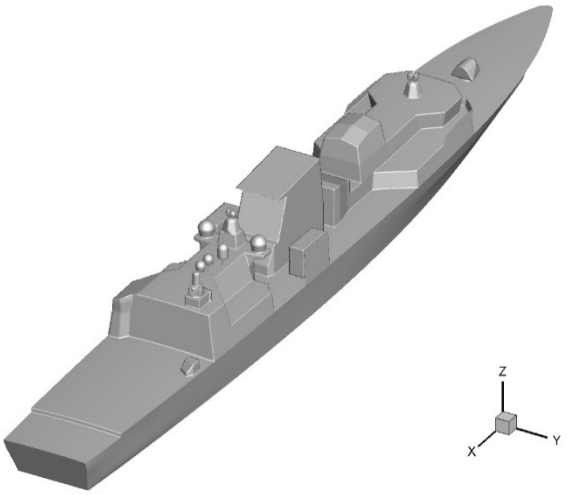

d) No-mast model

Figure 1. CPF models used in the present CFD study.

The freestream velocity U_∞ was set to 20 m/s in the computations because this speed corresponds to a mid-range wind speed for helicopter operations. The freestream turbulence intensity was set to 10% for the CFD simulations, which is comparable to the 9% measured in wind tunnel tests of the CPF model. In this study, computations were carried out for a headwind and a Red 20° wind condition (red winds are relative winds coming from the port side, green winds from the starboard side). Because of the complex multiple bluff body structures, numerical instabilities were encountered in computations when using the second-order central differencing scheme that was employed for the SFS2 geometry. Instead, a linear-upwind stabilized transport (LUST) scheme was used in computations for the no-mast case and a linear upwind scheme for the with-masts case. The computations were started from a uniform flow set as the freestream. A timestep of 1×10^{-3} seconds was used in the current CFD work, which resulted in a non-dimensional timestep $CFL_{max} \sim 4$ (detected at the masts rather than in the ship airwake). The computations were performed for 60 seconds of physical time, resulting in nine units of flow-through time (l_s/U_∞), with the last 50 seconds used for sampling. The computed results were compared with the available experimental wind tunnel data of a 1:50-scale CPF model. In the experiment, three points in the airwake (located starboard, port, and at mid deck in the CPF airwake, at a height and longitudinal location close to the rotor disc in high hover), were set up for velocity measurements using Cobra probes (Yuan et al., 2018a).

Table 1 shows computed results for both the with-masts and no-mast configurations using the linear-upwind scheme. Three probes were positioned in the middle of the airwake at a height and longitudinal location close to the rotor disc in high hover. Pitch and yaw angles are introduced to describe the flow directions in the body-axis coordinate system defined in **Figure 1**. The computations over-predicted the mean velocity at the starboard and mid-point locations. However, in general, the results of the with-masts configuration are closer to the experimental data. This comparison numerically confirms the effects of the masts. On the other hand, omitting the structures like masts may improve the numerical stability, and thus could allow the application of more accurate numerical schemes as a trade off. The mean velocity contained using the linear-upwind scheme for the no-mast configuration showed obvious discrepancies from the experimental data when compared with the LUST scheme, as expected, indicating that the numerical scheme plays a primary role in this study. Nevertheless, validation against at-sea and wind tunnel tests is the only way to check the adequacy of omission, depending on the focus of interest. Combined computational and experimental simulations provide a reliable means for real-world ship airwake investigations.

Table 1 Mean velocity magnitude (U/U_∞), pitch $\theta[^\circ]$, and yaw $\psi[^\circ]$ in CPF airwake with Red 20° wind

Approaches	1 (Starboard)			2 (Port)			3 (Mid)		
	U/U_∞	$\theta[^\circ]$	$\psi[^\circ]$	U/U_∞	$\theta[^\circ]$	$\psi[^\circ]$	U/U_∞	$\theta[^\circ]$	$\psi[^\circ]$
Experimental	0.56	-16.93	6.70	0.87	9.67	35.55	0.74	-4.02	33.35
Linear-upwind (with masts)	0.62	-11.27	7.43	0.69	6.21	26.19	0.93	2.65	27.48
Linear-upwind (no masts)	0.70	-13.00	14.09	0.66	7.96	26.79	1.02	1.83	25.71
LUST (no masts)	0.49	-14.16	-4.65	0.69	3.23	26.04	0.73	2.98	27.27

While quantitative differences in airwake results are the focus of this study, any small differences not affecting helicopter operations can be practically neglected. Studies with and without masts using the technology described in McTavish et al. (2015) indicate that the CPF masts have a negligible effect on helicopter operations. As a concluding remark, the mesh without masts has been used for the majority of CPF airwake flow analyses supporting helicopter landings onto and take-offs from the frigate deck.

3.2 Transient time period and time integration

The second challenge faced in CFD-aided ship design and helicopter operations was the long transient time period that needs to be removed for the final statistical analysis. Initial solutions can affect the flow field in the numerical simulations. Statistics are computed after the flow reaches a statistically stationary state. Conventionally, the flow-through time (c/U_∞) is used to help decide how to truncate the transient process, where c is a chord length of a representative airfoil. In the DNS performed by Shan et al. (2005) for a 2D NACA 0012 airfoil at 4 degrees, the amplitude of the velocity oscillations stayed at a certain level without significant change in time after the flow was established at $t = 10c/U_\infty$. In a large eddy simulation (LES) of flow around an airfoil near stall (Mary and Sagaut, 2002), around six time units were necessary to get a well-established unsteady solution from the initial steady Reynolds-averaged Navier-Stokes (RANS) solution, while the application of LES using a coarser mesh as an initial solution limited the initial transient to 1.5 time units. For averaging quantities, the averaging procedure was performed in the homogeneous spanwise direction and in time over a period of $2.4c/U_\infty$ in the work of Mary and Sagaut (2002).

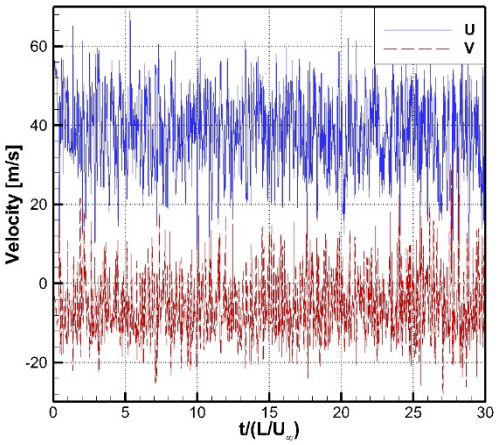

a) SFS2, velocity at a middle location over flight deck at a headwind condition

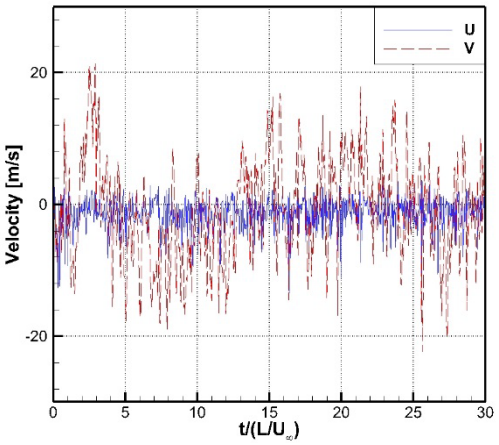

b) SFS2, velocity near intersection of the flight deck and hangar aft face

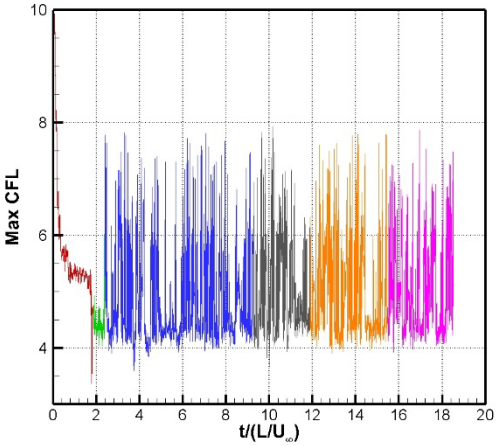

c) CPF, max. CFL number at Green 30°; colour lines distinguish computation runs

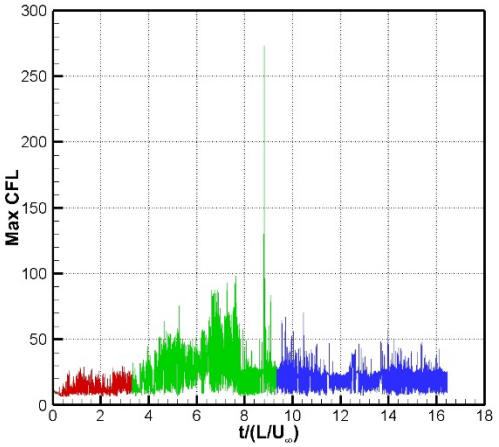

d) Canadian ship A, max. CFL at Green 30°; colour lines distinguish computation runs

Figure 2. Time histories of velocity.

In the SFS2 airwake study, Forrest and Owen (2010) used 2.3 flow-through time units (l_s/U_∞) to remove transients before unsteady sampling began, and the flow statistics were then averaged over the next 9 units of flow-through time. Extracting from the data published by Yuan et al. (2018a), **Figure 2**a and **Figure 2**b illustrate the time histories of the velocities at two locations in the SFS2 airwake, namely at a probe location at the middle over the flight deck, and at a location that is 15 cm (at full scale) away from the coordinate origin located on the centreline of the flight deck at the intersection of the flight deck surface and the aft face of the hangar. As can be seen in the figures, flow in the ship airwake reached a statistically stationary state after two units of flow-through time at the probe location. However, near the coordinate origin, the statistically dead flow did not reach a statistically stationary state until 15 flow-through time units. As a result, the statistical analysis was conducted by removing 16 time units. An alternative to evaluate if the simulation reached the statistically steady state is to check the maximum CFL number outputted by OpenFOAM. **Figure 2**c illustrates the time history of the maximum CFL number of the CPF, which indicates that the CPF simulation reached steady state after ~3 flow-through time units; however, this is configuration dependent. As shown in **Figure 2**d, the time history of the maximum CFL number of the CFD simulations conducted for an undisclosed Canadian ship (Canadian ship A in this study) reached steady state after ~9 flow-through time units, which is a long time period resulting in high CPU cost for the complex geometry. Since truncation of the transient period is configuration dependent, one has to check it case by case. Parallel computing is a practical mechanism to overcome the challenge of speeding up the computational time.

All the static computations reported so far were carried out on 64 processors using the parallelized OpenFOAM *pimpleFoam* solver. As the capability development turned to investigate complex ship configurations in production mode, the parallelization performance of the *pimpleFoam* solver had to be evaluated to manage the CFD simulations efficiently. An evaluation was conducted for the CPF, without masts, at 25 m/s. The mesh had 28.5 million control cells.

Table 2 summarizes the results of the evaluation tests. The use of 96 processors reduced the clock time of the computations by about 30% when compared with the nominal case using 64 processors. Additional processors added extra overhead due to the data transfer between the processors, and therefore the computations using 128 and 256 processors did not achieve a gain in speed-up efficiency or clock time. In addition, the use of more processors means decomposition of the computational domain into more subdomains, thus generating more decomposed matrices. Decomposed matrices cannot mathematically retain the same characteristics as the original matrix, possibly causing numerical instability in the computations or slower convergence.

Table 2 Efficiency of OpenFOAM parallelization for a test case of the CPF at headwind condition with 28.5 million cells

Processors	64	96	128	256
Physical time	0.2 s	0.2 s	0.2 s	0.2 s
Clock time	491 m	346 m	341 m	571 m
Speed up	1	1.42	1.44	0.86
Efficiency	100%	95%	72%	21%

The speedup factor divided by the ideal speedup (equal to the number of partitions) is the speedup efficiency. The parallel computing performance is case and facility dependent and for Canadian ship A, the parallel computing performance differed slightly (**Table 3** and **Table 4**). The meshes for the ship consisted of about 43.4 and 48.7 million cells, respectively. The clock time for each simulation was compared against the 64-

processor run data to estimate the total speedup factor. The performance revealed nearly linear scalability up to 160 processors. After 160 processors, the performance showed an obvious drop in speed-up efficiency. Nevertheless, parallel computing using more than 160 processors still achieved gains in speed up; 240 processors were used in a recent campaign supporting Canadian ship A design.

It should be noted that a critical issue connected to parallel computations in production mode is the license availability if commercial CFD software is used. OpenFOAM was selected for its cost effectiveness because it obviates the cost and restrictions, which CFD users encounter with commercial CFD software licenses.

Table 3 Efficiency of OpenFOAM parallelization for a test case of the Canadian ship A at headwind with 43.4 million cells

Processors	64	96	128	160
Physical time	4 s	4 s	4 s	4 s
Clock time	288393 s	197266 s	152428 s	124340 s
Speed up	1	1.46	1.89	2.32
Efficiency	100%	97.5%	94.6%	92.8%

Table 4 Efficiency of OpenFOAM parallelization for a test case of the Canadian ship A at R15° wind with 48.7 million cells

Processors	160	192	208	240
Physical time	1 s	1 s	1 s	1 s
Clock time	23939 s	23720 s	22115 s	19862 s
Speed up	1	1.01	1.08	1.2
Efficiency	100%	84%	83%	80%

3.3 Ship motion

Zan (2005) suspected that ship motion effects on the airwake could play an important role when large amplitude ship motions are present. The challenge for simulating flows past ships is to handle the mesh deformation around the complex ship geometry. Yuan et al. (2018b) used a solid-body mesh solver for the CPF in motion because a new capability using a radial basis function (RBF) added to OpenFOAM to compute motion-induced effects works currently only for oscillating airfoils. For illustration, the computed results are compared against representative wind tunnel and available sea-trial flight test data.

Wall et al. (2021) conducted wind-tunnel and sea-trial tests to investigate the airwake flows behind the CPF in motion. **Figure 3**a shows the setup of the CPF model in the wind tunnel and its ship-motion system in the test section. Spires placed at the entrance of the test section created a simulation of the atmospheric boundary layer. The frigate model was a 1:50-scale above-water model of the CPF. Three Cobra probes – starboard, centre, and port – were placed inline at a distance of 14 m at full scale from the hangar face. An additional Cobra probe was placed directly downstream of the centre probe. Five elevation configurations were investigated to survey the airwake, representing full-scale heights from 5.5 m to 9.5 m above the flight deck. The wind tunnel airwake measurements were acquired at a sampling rate of 5,000 Hz, with a low-pass filter frequency of 1,505 Hz. During a full-scale sea trial of the CPF, the flight deck was instrumented with four 10 m tall masts and each

mast was equipped with five 3D ultrasonic anemometers as shown in **Figure 3**b. Other reference anemometers and various logging equipment for ship motion, speed, and course, as well as ship anemometers were also installed on board.

Sinusoidal ship-motion profiles were used to understand the basic effects of motion resulting from a parametric variation in the amplitude and frequency of the motion. Simple sinusoidal profiles consisted of motion for one degree of freedom (one-DOF) only (heave, roll, or pitch). The motion frequency was 0.08 Hz at full scale. The amplitudes were 1.5 m for the heave, 3.4° for the pitch, and 5° for the roll conditions, respectively. Multi-DOF motions were measured as well, using combined sinusoidal profiles, which consisted of motion for two- or three-DOF; realistic profiles were also developed by DRDC using typical seaway characteristics. Some of the preliminary results were published in Yuan et al. (2018b).

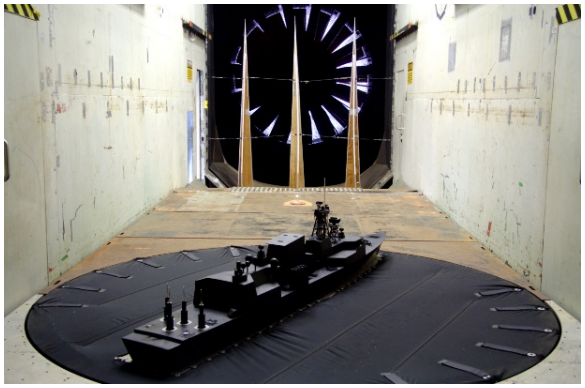

a) Setup of the oscillating CPF model in the wind tunnel

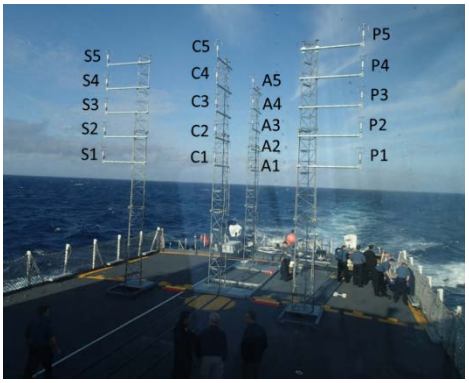

b) Corresponding anemometer support masts on flight deck at sea trial

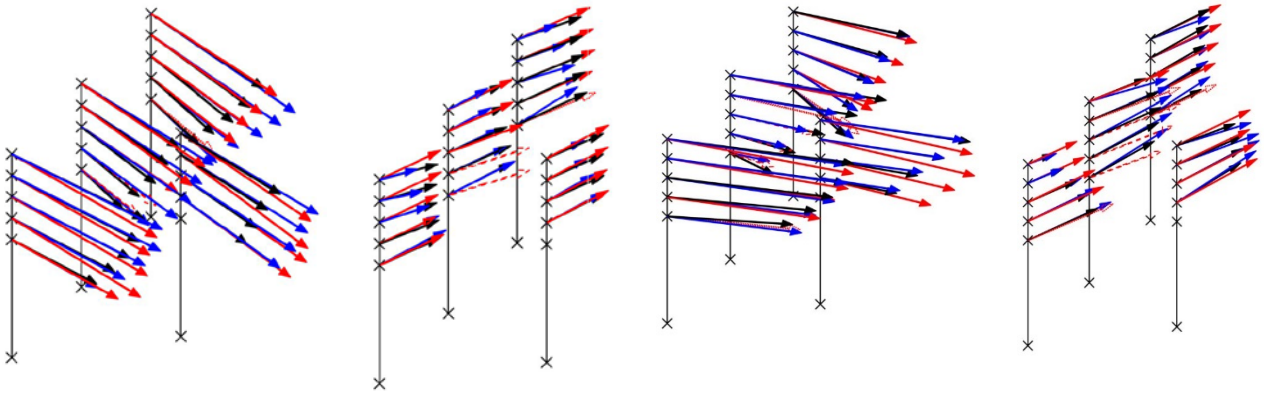

Mean velocity **Standard deviation** **Mean velocity** **Standard deviation**

1) Headwind **2) Red 15° wind**

c) **Mean velocity vector and standard deviation in the CPF flight deck wake for roll conditions; red – wind tunnel, blue – CFD, black – sea trial**

Figure 3. Combined experimental and computational investigation of the CPF in motion.

The airwake of the CPF was investigated using combined in-house experimental and computational simulations as discussed above. **Figure 3**c illustrates the velocity vectors and their standard deviations in the CPF flight deck wake at the locations as indicated in **Figure 3**a and **Figure 3**b when the ship was in roll motion. In general, the validation between methods demonstrated consistent trends and reasonable accuracy in computed values,

all of which indicate that the CFD (and wind tunnel) results represent this shipboard environment for the purposes as adopted in Canada.

Table 5 compares selected computed results against equivalent experimental wind tunnel data, in terms of the mean values of the normalized flow velocity magnitude, pitch, and yaw, and their fluctuations. In general, the computed results compared well to the experimental data for both static and motion conditions, although the CFD results showed less unsteadiness than the experimental results did. With the exception of flow unsteadiness, which must be higher to achieve the appropriate level of fidelity, the level of agreement shown in the table is consistent with the desired level.

Table 5 reveals that the ship motion intensified the flow fluctuations over the flight deck, in both magnitude and direction (pitch and yaw), with the strongest influence due to the ship pitch motion. The relative discrepancy between the CFD and wind tunnel data is not consistent, which may provide insight into the strengths and weaknesses of the different computational approaches under development. **Table 5** also shows that oblique wind angles amplified the flow directional fluctuations in the airwake over the flight deck.

Table 5 Mean velocity and fluctuations of velocity in the airwake over the flight deck behind the CPF in motion, at location C5 in Figure 3c – the highest elevation (z = 9.5 m) of the centre probe (x = 14 m)

Condition	Motion	U/U_∞		θ[°]		ψ[°]		U'/U_∞		θ'[°]		ψ'[°]	
		CFD	Exp	CFD	Exp	CFD	Exp	CFD	Exp	CFD	Exp	CFD	Exp
Headwind	Static	0.76	0.76	-9.01	-8.66	0.41	-3.44	0.09	0.16	5.41	9.09	7.41	12.15
Headwind	Heave	0.77	0.76	-9.45	-8.66	0.26	-2.73	0.10	0.16	5.54	9.03	6.77	12.21
Headwind	Pitch	0.63	0.76	-11.07	-8.85	1.86	-2.61	0.23	0.17	10.61	9.08	12.93	12.06
Headwind	Roll	0.78	0.76	-9.83	-8.53	0.44	-2.41	0.09	0.15	4.75	8.86	8.01	12.00
Red 15°	Heave	0.79	0.84	1.88	-1.32	22.41	21.23	0.18	0.21	11.53	11.01	13.72	13.24
Headwind	Heave-Pitch	0.72	0.76	-9.77	-8.51	0.72	-2.78	0.15	0.16	6.38	9.16	8.31	12.24
Headwind	Heave-Roll	0.76	0.76	-9.29	-8.67	0.39	-3.32	0.11	0.16	5.99	9.23	7.76	12.36

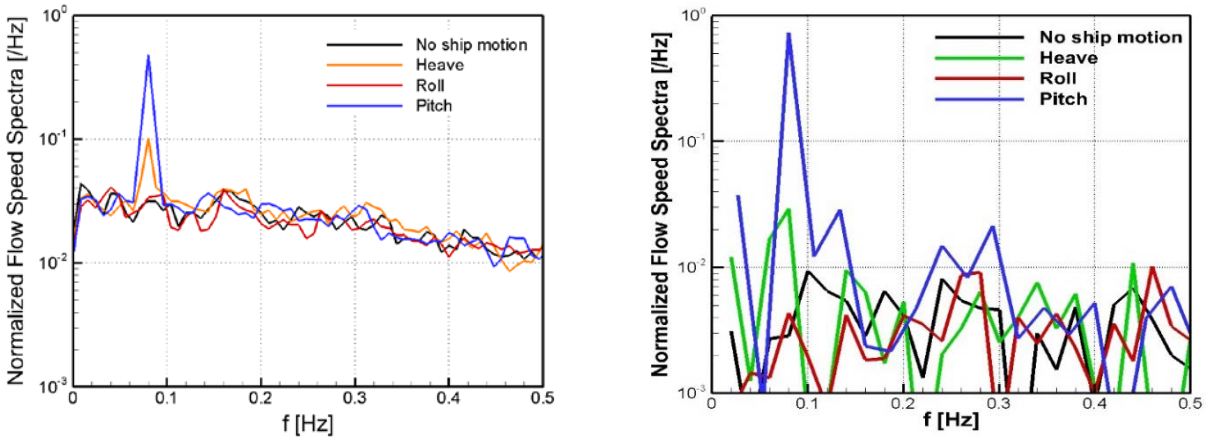

Experimental **Computed**

Figure 4. Effect of ship motion on airwakes – spectra of a probe in the airwake middle at the height of the rotor plane in helicopter high hover, adopted from Yuan et al. (2018b).

Figure 4 shows the differences in the spectra of the centre probe at the height of the rotor plane in helicopter high hover for three simple sinusoidal cases: heave, roll, and pitch. The spectra of the flow speed magnitudes showed periodic responses at the motion frequency. Pitch motion had the most significant impact on the airwake, while heave had lesser and roll had minimal impact at headwind conditions. Although the computed magnitude of the oscillations were higher, the current CFD predicted similar trends, which are comparable to the experimental ones, with lower overall energy, consistent with the results in **Table 5**. It is believed that the spectra will be more accurate with longer time series.

4.0 APPLICATION OF CFD DATA TO PILOTED FLIGHT SIMULATORS

Ship airwake CFD results are used for a number of different types of analysis in Canada. However, one of the most powerful applications is using them for high-fidelity piloted flight simulation in shipboard environments. For simulator applications, CFD results could be used in two ways. The physics-based approach would allow the CFD to calculate the forces on the simulated aircraft by consulting a look-up table of the flow information. Nevertheless, engineering models could also be used to simplify the determination of the forces on the aircraft, as detailed below.

4.1 Flight simulator look-up table

The unsteady CFD simulations produced large quantities of time-varying data for airwake velocities. It is challenging to save the unsteady flow quantities for the entire flight deck for all of the timesteps. Practically, solutions are stored as a look-up table in an "extraction box", as demonstrated in **Figure 5**, which is a predetermined regular grid where a certain time series is stored for each grid point. Typically, airwake data is solved for a certain number of seconds and then that data is played back in a loop with smoothing to keep the data set a manageable size. In order for look-up tables to work appropriately, the helicopter rotor modelling must be of sufficient fidelity to include changing wind measurements across the rotor at each simulation time step. In general, this means that the rotor models require multiple elements per blade where aerodynamic forces are calculated. Not all simulator-ready aircraft models include this capability.

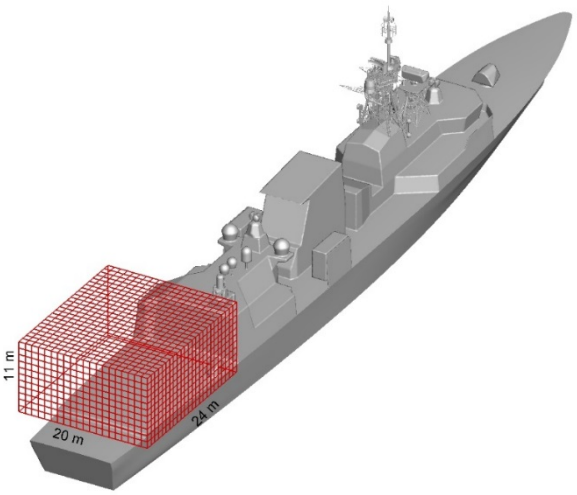

Figure 5. CPF extraction box for the flight simulator look-up tables.

Figure 6 compares the flowfield with a headwind for the selected portside planes in the ship airwake, which cross-check the data within the extracted box. When compared with particle image velocimetry (PIV) results, the computed results capture the major features of the flow. For the headwind case, a reduction in longitudinal velocity can be seen near the centre, within the wake behind the hangar. Significant gradients exist in the time-averaged values of the velocity components, which would affect the trim of the helicopter. The CFD-predicted separation zone was slightly smaller than what is shown in the PIV results. The results from CFD configurations both with and without the masts are reasonably comparable. The flow field for Red 20° wind were reported in Yuan et al. (2018b). This test case was much more challenging because the oblique wind intensifies the complexity of the separated flow. Nevertheless, the CFD results matched the PIV results well in general. The velocity deficit and gradients were reasonably predicted. The prediction of the separation zone using the no-mast configuration was even better than that observed for the with-masts case. This was mainly attributed to the applied numerical scheme.

Figure 6. CPF airwake data, longitudinal mean flow, headwind, flow from right to left, dimensions in meters, the coordinate origin is located on the centreline of the flight deck at the intersection of the flight deck surface and the aft face of the hangar.

4.2 Airwake load modelling for flight simulation

Using CFD to expand the helicopter loading model relies on the idea that the unsteadiness in the flow field, averaged over some target area, is related to the helicopter unsteady loads. This concept was previously introduced by McTavish et al. (2015), where an experimental apparatus for measuring helicopter unsteady loads, particularly rotor loads, was introduced, and results comparing rotor loads and average flow turbulence were given.

In situations where the simulator model does not include the ability to calculate complex loading from time-accurate CFD solutions, the airwake properties could be converted to overall aircraft loading using engineering models relating loading and airwake properties. As such, the results of a complex airwake could be applied to an aircraft model as a resultant load requiring only one vehicle element in the simulator model. To preserve the unsteady nature of the loading, a method such as the Advancing Fourier Series method developed by Wall et al. (2013) could be used.

Using recent CFD results, this relationship was investigated by comparing unsteady rotor loads and the average turbulence as calculated from the CFD results in a rectangular volume approximately encompassing the rotor

disc area. **Figure 7** shows the relationship for a number of different wind directions (left plot) and helicopter positions (right plot). The figure shows the vertical unsteady force versus the unsteady flow quantity in groups corresponding to different wind speeds (each line) for different rotor positions (line type) and wind directions (line colour).

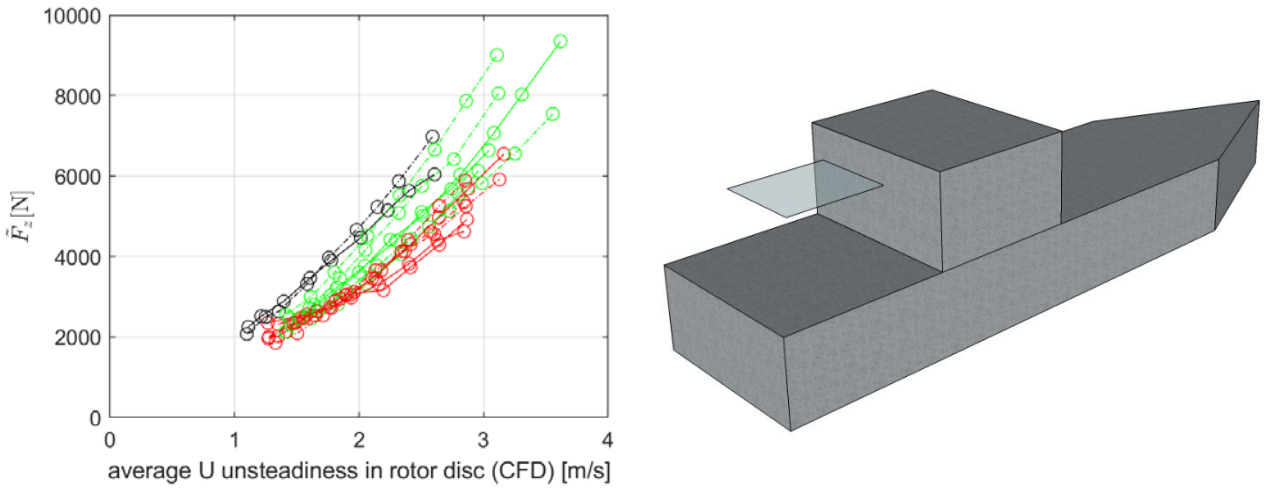

Figure 7. Relationship between unsteady loads and computed turbulence on rotor disc planes.

5.0 CONCLUSIONS

In this study, a high-fidelity CFD capability was developed to aid Canadian industry and defence ship design and offshore helicopter safe operation. The open-source CFD tool OpenFOAM was validated for computations of three-dimensional unsteady incompressible ship airwake flows behind the real-world CPF frigate. Applying DDES to model the turbulence, the computed results showed reasonable agreement at an acceptable level with the wind tunnel data, demonstrating the ability of OpenFOAM and the DDES model to capture important features in unsteady ship airwake flows.

Combined computational and experimental simulations provided a reliable means for real-world ship airwake investigations, supporting Canadian industrial and navy flight simulator development and application. The computational and experimental simulations showed a typical reduction in velocity within the wake behind the hangar and significant gradients in the velocity components, which are known to affect helicopter operations.

There exist challenges when applying the developed CFD capability to real-world industrial and defence flight simulations. Having addressed the challenges, corresponding measures and lessons learned during the course of the capability development were discussed and recommended in detail, with the goal of supporting industrial and defence ship design and helicopter operations.

REFERENCES

[1] Ferziger, J. H., and Perić, M. *Computational Methods for Fluid Dynamics*, Springer-Verlag, Berlin, 1996.
[2] Forrest, J, and Owen, I. An Investigation of Ship Airwakes using Detached-Eddy Simulation. *Computers & Fluids*, Vol. 39, pp. 656–673, 2010.
[3] Forrest, J., Owen, I., Padfield, G., and Hodge, S. Ship–Helicopter Operating Limits Prediction Using Piloted Flight Simulation and Time-Accurate Airwakes. *Journal of Aircraft*, Vol. 49, No. 4, pp 1020-1031, 2012.

[4] Hodge, S., Forrest, J., Padfield, G., and Owen, I. Simulating the Environment at the Helicopter-ship Dynamic Interface: Research, Development and Application. *The Aeronautical Journal*, Vol. 116, No. 1185, pp. 1155-1184, 2012.
[5] Mary, I., and Sagaut, P. Large Eddy Simulation of Flow around an Airfoil near Stall. *AIAA Journal*, Vol. 40 No 6, pp. 1139-1145, 2002.
[6] McTavish, S., Wall A., Lee R. A Methodology to Correlate Simulated Airwake Data and Unsteady Helicopter Load Measurements to Shipboard Helicopter Fight Test Data. *14th International Conference on Wind Engineering*, 2015.
[7] OpenFOAM. The Open Source CFD Toolbox. *User Guide*, Version 2.3.0, Feb. 2014.
[8] Owen I., Lee R., Wall A., and Fernandez N. The NATO Generic Destroyer - a Shared Geometry for Collaborative Research into Modelling and Simulation of Shipboard Launch and Recovery. *Ocean Engineering*, Vol. 228, 2020.
[9] Polsky, S. Application and Verification of Sub-Grid Scale Boundary Conditions for the Prediction of Antenna Wake Flowfields. *5th International Colloquium on Bluff Body Aerodynamics and applications*, Ottawa, Canada, July 11-15, 2004.
[10] Polsky, S. Progress towards Modeling Ship/Aircraft Dynamic Interface. *HPCMP Users Group Conference*, IEEE Computer Society, 2006.
[11] Polsky, S. NAVAIR Airwake Modeling & More. *HPC User Group Forum*, 2008.
[12] Polsky, S. and Wilkinson, C. A Computational Study of Outwash for a Helicopter Operating near a Vertical Face with Comparison to Experimental Data. *AIAA Modeling and Simulation Technologies Conference*, Chicago, Illinois, AIAA 2009-5684, August 10-13, 2009.
[13] Shan, H., Jiang, L., and Liu, C. Direct numerical simulation of flow separation around a NACA 0012 airfoil. *Computers & Fluids*, Vol. 34, pp. 1096–1114, 2005.
[14] Spalart, P. R., Deck, S., Shur, M. L., Squires, K. D., Strelets, M. K., and Travin, A. A New Version of Detached-eddy Simulation, Resistant to Ambiguous Grid Densities. *Theoretical and Computational Fluid Dynamics*, Vol. 20, No. 3, pp. 181-195, 2006.
[15] Wall A., Lee R., and Barber H., Thornhill E. *The NATO Generic Destroyer - a Shared Geometry for Collaborative Research into Modelling and Simulation of Shipboard Launch and Recovery: Source Data*. Open Science Canada, https://open.canada.ca/data/en/dataset/2c30e366ef2b-400e-8363-0b13e4a7b6f4; 2020.
[16] Wall, A., Thornhill, E., Barber, H., McTavish, S. and Lee, R. Experimental Investigations into the Effect of At-sea Conditions on Ship Airwake Characteristics. Submitted to *Journal of Wind Engineering and Industrial Aerodynamics*, 2021.
[17] Wall, A., Zan, S., Langlois, R. and Afagh, F. Correlated Turbulence Modelling: An Advancing Fourier Series Method. *Journal of Wind Engineering and Industrial Aerodynamics*, vol. 123, pp155-162, 2013.
[18] Wilkinson, C.H., Zan, S.J., Gilbert, N.E., and Funk, J.D. Modeling and Simulation of Ship Air Wakes for Helicopter Operations – A Collaborative Venture. *Symposium on Fluid Dynamics Problems of Vehicles Operating near or in the Air-Sea Interface*, Amsterdam, Netherlands, October. NATO RTO-MP-15, pp 8-1 to 8-12, 1998.
[19] Yuan, W., Wall, A., and Lee, R. Combined Numerical and Experimental Simulations of Unsteady Ship Airwakes. *Computers & Fluids*, Vol. 172, pp. 29-53, 2018a.
[20] Yuan, W., Wall, A., and Lee, R. Simulations of Unsteady Airwakes behind Ships in Motion. *31st Congress of the International Council of the Aeronautical Sciences*, Belo Horizonte, Brazil, 09-14 September, 2018b.
[21] Zan, S. On Aerodynamic Modelling and Simulation of the Dynamic Interface. *Proc Inst Mech Eng, Part G: J Aerospace Eng*, Vol. 219, No. 5, pp. 393–410, 2005.